Canard-induced complex oscillations in an excitatory network

Elif Köksal Ersöz, Mathieu Desroches, Antoni Guillamon, Joel Tabak, John Rinzel

▶ **To cite this version:**

Elif Köksal Ersöz, Mathieu Desroches, Antoni Guillamon, Joel Tabak, John Rinzel. Canard-induced complex oscillations in an excitatory network. Journal of Mathematical Biology, In press, 10.1007/s00285-020-01490-1 . hal-01939157v1

HAL Id: hal-01939157

https://inria.hal.science/hal-01939157v1

Submitted on 29 Nov 2018 (v1), last revised 31 Mar 2020 (v2)

HAL is a multi-disciplinary open access archive for the deposit and dissemination of scientific research documents, whether they are published or not. The documents may come from teaching and research institutions in France or abroad, or from public or private research centers.

L'archive ouverte pluridisciplinaire **HAL**, est destinée au dépôt et à la diffusion de documents scientifiques de niveau recherche, publiés ou non, émanant des établissements d'enseignement et de recherche français ou étrangers, des laboratoires publics ou privés.

Canard-induced complex oscillations in an excitatory network

E. Köksal Ersöz[1,2], M. Desroches[1,2], A. Guillamon[3], and J. Tabak[4]

[1]MathNeuro Team, Inria Sophia Antipolis Méditerranée, Valbonne, France
[2]Université Côte d'Azur, France
[3]Universitat Politècnica de Catalunya, Departament de Matemàtiques, Barcelona, Spain
[4]University of Exeter Medical School, University of Exeter, Exeter, UK

November 28, 2018

Contents

1 Introduction **2**

2 Canard-mediated transitions to burst and spike-adding in the (a, d, θ)-model **5**

3 Folded node and MMOs in the (a, θ, s)-model **8**

3.1 MMOs and behaviour along isolas 13

4 Canard-mediated MMBOs oscillations in the (a, d, θ, s)-model **14**

4.1 MMBOs and behaviour along isolas 18

5 Conclusion **20**

1 Introduction

Complex oscillatory patterns arising in Neuroscience (excitability, spiking, bursting and subthreshold oscillations) have been intensively studied via mathematical modelling at multiple spatial and temporal scales, ranging from single cell to network level. These complex dynamics occur due to strong interaction of system variables across various timescales. Multiple timescale (so-called *slow-fast* or *singularly perturbed*) dynamical systems provide an efficient ground to study those patterns [12, 16].

In slow-fast dynamical systems, the timescale separation parameter ε is a small scalar quantity ($0 < \varepsilon \ll 1$) that measures the speed difference between the state variables. The presence of ε results in having distinct groups of slow and fast variables, and the overall dynamical behaviour of the system can be divided into slow and fast epochs. In its most general form, a slow-fast system can be written as follows:

$$\begin{aligned} \mathbf{x}' &= \mathbf{f}(\mathbf{x}, \mathbf{y}, \varepsilon), \\ \mathbf{y}' &= \varepsilon \mathbf{g}(\mathbf{x}, \mathbf{y}, \varepsilon), \end{aligned} \tag{1}$$

where $\mathbf{x} \in \mathbb{R}^n$ is the vector of fast variables, $\mathbf{y} \in \mathbb{R}^m$ is the vector of slow variables and the prime denotes differentiation with respect to the fast time τ; the functions $\mathbf{f}$ and $\mathbf{g}$ are assumed to be sufficiently smooth. Setting $\varepsilon = 0$ in (1) freezes the dynamics of the slow variables in $\mathbf{y}$ and gives the *fast subsystem* (so-called *layer problem*), which describes the dynamics of the fast variables in $\mathbf{x}$ for fixed values of the slow variables (now parameters) and, hence, approximates the dynamics of the original system during fast epochs.

Applying the time rescaling $t = \varepsilon\tau$ gives the slow-time parametrisation of the original system, which reads:

$$\begin{aligned} \varepsilon \dot{\mathbf{x}} &= \mathbf{f}(\mathbf{x}, \mathbf{y}, \varepsilon), \\ \dot{\mathbf{y}} &= \mathbf{g}(\mathbf{x}, \mathbf{y}, \varepsilon). \end{aligned} \tag{2}$$

Taking $\varepsilon = 0$ in (2) yields the *slow subsystem* (so-called *reduced system*), which is a set of differential equations on the slow variables $\mathbf{y}$ constrained by the algebraic condition $\mathbf{0} = \mathbf{f}(\mathbf{x}, \mathbf{y}, 0)$. This algebraic equation defines the *critical manifold* $S^0 := \{\mathbf{f} = \mathbf{0}\}$, which then corresponds to both the phase space of the slow subsystem and to the set of the equilibria of the layer problem.

The stability of the layer problem's equilibria determines whether subsets of the critical manifold can be said to be attracting, repelling or of saddle type. More generally, hyperbolic equilibria of the layer problem correspond by definition to so-called *normally hyperbolic* points of S^0. This provides the key assumption for the persistence of compact submanifolds of S^0 (which are invariant for $\varepsilon = 0$) as locally invariant manifolds of the original system for small enough $\varepsilon > 0$. Indeed, Fenichel theory [14] guarantees the existence of locally invariant (attracting, repelling or saddle-type) slow manifolds S^ε as perturbations of compact normally hyperbolic (attracting, repelling or saddle-type) submanifolds of S^0.

Attracting and repelling branches of S^0 (S^a and S^r, respectively) meet along the *fold set*

$$F := \{(\mathbf{x}_{\text{fold}}, \mathbf{y}_{\text{fold}}) \in S^0;\ (D_{\mathbf{x}}\mathbf{f}(\mathbf{x}_{\text{fold}}, \mathbf{y}_{\text{fold}}, 0)) = \mathbf{0}\},$$

which corresponds to a saddle-node bifurcation set of the layer problem. Since normal hyperbolicity is lost at every point of F, Fenichel theory does not apply and different mathematical techniques must be employed in order to understand the dynamics of the original system near F. The usual strategy is to analyse the slow flow (2) in the singular limit $\varepsilon = 0$ by differentiating S^0 with respect to time, giving

$$\begin{aligned} -\det(D_{\mathbf{x}}\mathbf{f})\dot{\mathbf{x}} &= (\operatorname{adj}(D_{\mathbf{x}}\mathbf{f}) \cdot D_{\mathbf{y}}\mathbf{f} \cdot \mathbf{g})(\mathbf{x}, \mathbf{y}, 0), \\ \dot{\mathbf{y}} &= \mathbf{g}(\mathbf{x}, \mathbf{y}, 0), \end{aligned}$$

where $\operatorname{adj}(D_{\mathbf{x}}\mathbf{f})$ denotes the adjugate of the matrix $D_{\mathbf{x}}\mathbf{f}$. This system is singular on the fold points when $\det(D_{\mathbf{x}}\mathbf{f}) = 0$. To overcome the singularity problem, one can use a rescaling factor $\det(D_{\mathbf{x}}\mathbf{f})$

and obtain the so-called *desingularized reduced system* (DRS), whose equations take the form:

$$\begin{aligned} \mathbf{x}' &= (\mathrm{adj}(D_{\mathbf{x}}\mathbf{f}) \cdot D_{\mathbf{y}}\mathbf{f} \cdot \mathbf{g})(\mathbf{x}, \mathbf{y}, 0), \\ \mathbf{y}' &= -\det(D_{\mathbf{x}}\mathbf{f})\mathbf{g}(\mathbf{x}, \mathbf{y}, 0). \end{aligned} \tag{3}$$

Equilibria of the DRS satisfying $\det(D_{\mathbf{x}}\mathbf{f}) = 0$ are called *folded equilibria* or *folded singularities* of the original system. Hence, saddle, node and saddle-node equilibria of the DRS give *folded-saddle*, *folded-node* and *folded-saddle-node* singularities, respectively. Folded singularities are dynamically interesting objects mainly because they are known to give rise to *canard solutions*. A canard is a solution of a slow-fast system which flows successively near S^a towards S^r, by passing close to a folded singularity, which in planar systems is called a *canard point* [2, 22]. Note that folded foci do exist but are much less interesting as they do not give rise to canards.

Canard dynamics are relevant in Neuroscience as canard solutions occur in a large class of neuron models, starting with the planar ones. The canard phenomenon in two-dimensional (2D) slow-fast systems explains the sharp transition, upon parameter variation, from equilibria (resting states in the neuronal context) to relaxation cycles (action potentials or spikes). This sharp increase in the cycle amplitude (referred to as a *canard explosion*) occurs within an exponentially small (in ε) parameter range and it is in particular observed in the van der Pol (VDP) system, which can be seen as a caricature of a type-II excitable neuron[1]. In VDP type systems, the critical manifold is one-dimensional and S-shaped: it has two attracting (external) branches separated by a repelling branch. In such systems, *canards without head* solutions correspond to limit cycles with segments on one of two attracting branches of the critical manifold and on the repelling branch; on the other hand, *canard with head* solutions correspond to limit cycles with segments on two attracting branches of the critical manifold and on the repelling branch. These two families of canard cycles are connected in parameter space by the so-called *maximal canard*, which by definition is the limit cycle solution with the longest repelling segment. In the neuronal context, the maximal canard provides the best approximation of the excitability threshold for type-II neurons and hence stands as a clear boundary between subthreshold oscillations (corresponding to canards without head) and spiking solutions (corresponding to canards with head and then to relaxation cycles) [7, 10, 24]. The role of canards in the synchronisation of 2D excitable systems has recently started to be unveiled [18, 19].

In three-dimensional (3D) slow-fast systems, canards play a similar crucial role in approximating firing thresholds [23] and in organising complex oscillations, such as *mixed mode oscillations* (MMOs) and *bursting* oscillations. MMO-type solutions combine small-amplitude oscillations (SAOs) and large-amplitude oscillations (LAOs) of relaxation type, in a recurrent (periodic or not) fashion. They arise in 1 fast/ 2 slow systems possessing a folded-node or a folded-saddle-node singularity. Such MMO systems can be interpreted as canard oscillators (of VDP type) with a drift that allows to flow through the canard point of the associated canard oscillator, and a global reinjection mechanism ensuring that these dynamics recur [5, 40]; see the review article [8] for details. In neuronal models, the appearance of subthreshold oscillations and subsequent transitions to spikes can be governed by an underlying canard structure [17, 21, 32, 33].

Another way to extend a planar slow-fast system to a 3D one is to have 2 fast and 1 slow variables; this can give a different type of slow-fast oscillations termed as *bursting oscillations*. Bursting oscillations correspond to fast oscillations (that is, in the neuronal context, a sequence of spikes) followed by a quiescent phase during which the system is slowly evolving. Most burster are 2 fast/1 slow systems and their 2D fast subsystems are bistable oscillators where the bistability is typically between limit cycles and equilibria.

The classical interpretation of bursting oscillations as recurrent slow-fast transitions between quiescence and burst is due to Rinzel [29, 30, 31], who had the seminal idea to relate such transitions to bifurcations of the fast subsystem. In the full system, these transitions are then the result of a slow drift through relevant fast subsystem bifurcations since the parameter displaying these bifurcations is the slow variable. Based on this idea, Rinzel came up with a classification of bursting patterns

[1]Neurons are said to have type-II excitability when they cannot fire action potentials below a positive minimal frequency; from the modelling standpoint they correspond to systems operating near a Hopf bifurcation [12].

that include three classes (*square-wave*, *elliptic*, *parabolic*); see [29, 30, 31] for details. As proposed by Izhikevich in [16], one can further classify many types of bursting oscillations by identifying in each class one fast subsystem bifurcation (typically of equilibria) responsible for the quiescence-to-burst transition in the full system, and another fast subsystem bifurcation (typically of limit cycles) responsible for the burst-to-quiescence transition in the full system.

Terman identified a spike-adding phenomenon in a square-wave burster built upon the Morris-Lecar spiking model with an additional slow variable [38]. This slow-fast phenomenon involves canard trajectories organising spike-adding transitions and saddle-type slow manifolds; since then it has been found in a number of bursting models [9, 11, 15, 25, 28, 39]. These studies also revealed that canards play a similar role in the transition from rest to bursting in (at least) 3D slow-fast systems as they do in the transition from rest to spiking in planar systems. Another canard structure in spiking-bursting transitions is *torus canards* [6, 20].

MMO and bursting dynamics can be combined within the framework of four-dimensional (4D) systems with 2 slow and 2 fast variables. The resulting complex oscillatory dynamics has been termed as *mixed mode bursting oscillations* (MMBOs) [9]. MMBO-type complex oscillations arise due to a slow passage through a spike-adding canard explosion in certain types of bursting systems where the burst is initiated through a saddle-node bifurcation of the fast subsystem. Desroches et al. [9] described MMBOs in an extended version of the Hindmarsh-Rose system with a slowly-varying external input. They also discussed the presence of these dynamics in the Morris-Lecar-Terman system [38] and a biological modelling of secreting neurons [3].

MMBOs are the main focus of the present article. In what follows, we study a model of spontaneous episodic activity of developing spinal cord of the chick embryo, developed and analysed in [13, 26, 27, 37, 36, 35]. This episodic activity is composed of active phases of network spikes followed by quiescent periods. Following experimental observations [13, 26, 27], Tabak et al. have modelled the network activity using a rate model formalism with activity-dependent network depression and the assumption of excitatory connectivity between underlying neurons. To this end, they introduced two fast (a, d) and two slow (s, θ) variables, which represent the activity (population activity or mean firing rate) (variable a), the fraction of synapses not affected by the fast synaptic depression (d), the fraction of synapses not affected by the slow synaptic depression (s) and the threshold for the cell firing θ, respectively. The resulting 4D system reads:

$$\begin{aligned}
\tau_a \dot{a} &= a_\infty(w\, d\, s\, a - \theta - \theta_0) - a,\\
\tau_d \dot{d} &= d_\infty(a) - d,\\
\dot{\theta} &= \varepsilon(\theta_\infty(a) - \theta),\\
\dot{s} &= \varepsilon\tilde{\tau}_s(s_\infty(a) - s),
\end{aligned} \tag{4}$$

with sigmoid functions:

$$\begin{aligned}
a_\infty(v) &= 1/\left(1 + \mathrm{e}^{-(v)/k_a}\right),\\
d_\infty(a) &= 1/\left(1 + \mathrm{e}^{(a-\theta_d)/k_d}\right),\\
\theta_\infty(a) &= 1/\left(1 + \mathrm{e}^{-(a-\theta_\theta)/k_\theta}\right),\\
s_\infty(a) &= 1/\left(1 + \mathrm{e}^{(a-\theta_s)/k_s}\right).
\end{aligned} \tag{5}$$

Tabak et al. considered various 3D subsystems of (4) in order to study different aspects of the dynamics. The (a, d, θ)-model (where s does not appear in the a-equation) and the (a, d, s)-model (where θ is a parameter) reproduce the experimentally observed bursting behaviour [37]: the slow variables θ (in the (a, d, θ)-model) and s (in the (a, d, s)-model) control the periodic transitions between the active (fast oscillations due to the interaction between a and d) and the silent phase. On the other hand, the (a, θ, s)-model [35] does not account for the fast synaptic kinetics but instead captures the impact of the cellular excitability and the network connectivity on the durations of the active and silent phases of the episodic activity. The resulting behavior of the (a, θ, s)-model is a relaxation cycle in the 3D phase space.

Although these 3D reductions help to understand the effects of underlying biological variables on the network activity, they reproduce most of the features of the network activity. However, the fluctuations between the active phases were interpreted as noise. On the other hand, by looking carefully at the panel C of Figure 9 in [37], one could interpret the quiescent dynamics as oscillatory rather than being the result of noise. These type of complex oscillations – subthreshold oscillations followed by a bursting regime – fall into the category of MMBO-type solutions. The aim of the present study is to reproduce such complex oscillations by considering the (a, d, θ, s)-model (4). Figure 1 shows an example of MMBO-type trajectory produced by system (4). Throughout the paper, we shall use the parameter set given in [37], also provided in the caption of Figure 1, leaving the network connectivity measure w as the main bifurcation parameter; see [37] for detailed description of the parameters.

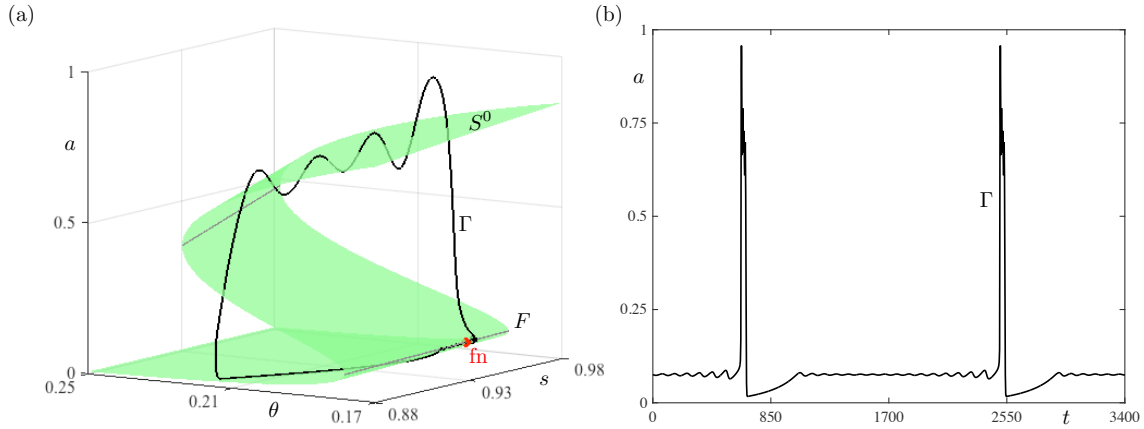

Figure 1: System (4) with $w = 1.43$ and $\tau_a = 1$, $k_a = 0.05$, $\tau_d = 2$, $\theta_d = 0.2$, $k_d = 0.5$, $\varepsilon = 1/\tau_\theta = 1/1000$, $\theta_\theta = 0.15$, $k_\theta = 0.05$, $\tilde{\tau}_s = \tau_\theta/\tau_s = 2$, $\theta_s = 0.14$, $k_s = 0.02$, $\theta_0 = 0$. (a) MMBO solution Γ projected onto the (θ, s, a)-space. Also shown are the critical manifold S^0, the fold curve F and the folded node fn (red dot). (b) Time profile of Γ for the a-variable.

In this study, we focus on the canard structures and associated canard-mediated dynamics in the 4D rate model (4) as well as in its two aforementioned reductions, and their impact on the complex oscillatory activity of the network. In Section 2, we detail the canard-mediated spike-adding transitions in the bursting regime of the (a, d, θ)-model. In Section 3, we unveil and analyse MMO dynamics in the (a, θ, s)-model. Then, in Section 4, we explain how to combine the bursting dynamics of the (a, d, θ)-model and the MMO dynamics of the (a, θ, s)-model into MMBOs using the (a, d, θ, s)-model. Finally, in Section 5, we summarise our findings, their relevance to the neural system under investigation and propose further avenues of research in this direction.

2 Canard-mediated transitions to burst and spike-adding in the (a, d, θ)-model

Tabak et al. considered two 3D reductions of the (a, d, θ, s)-model with 2 fast/1 slow variables, the (a, d, θ) and (a, d, s) models [37]. In both systems, the fast variables, a and d, form a bistable system of oscillations and equilibria parameterised by the cellular threshold θ and the activity-dependent depression s, respectively. Slow modulations in θ in the (a, d, θ)-model and s in the (a, d, s)-model govern recurrent dynamic transitions in the full 3D system between the oscillatory and stationary states of the (a, d) fast subsystem, which result in the bursting behaviour.

Canard-induced dynamics in bursting systems has been unveiled in several models [9, 11, 15, 25, 28, 38, 39], where bursting is initiated, upon parameter variation, via a Hopf bifurcation followed by a sequence of canard explosions and spikes are shaped via canard trajectories. In this section we investigate canard-induced dynamics in the (a, d, θ)-model keeping s as the bifurcation parameter. We use the same parameter set for which MMBO solutions exists in (4) (Figure 1 and Section 4), but

change $\tau_\theta = 5000$ for a clear visualisation of transitions. Note that similar study in the (a, d, s)-model with the parameter θ will give qualitatively similar slow-fast transitions.

The (a, d, θ)-model reads:

$$\begin{aligned} \tau_a \dot{a} &= a_\infty(w\, d\, s\, a - \theta - \theta_0) - a, \\ \tau_d \dot{d} &= d_\infty(a) - d, \\ \dot{\theta} &= \varepsilon(\theta_\infty(a) - \theta), \end{aligned} \tag{6}$$

where $\varepsilon = 1/\tau_\theta$ being the small parameter (given that $\tau_a = 1$ and $\tau_d = 2$). System (6) undergoes a supercritical Hopf bifurcation at $s_{Hopf} \approx 0.95657$. As in the canard explosion scenario in planar systems, the canard solutions of (6) lie along a quasi-vertical segment of the solution branch in the bifurcation diagram in terms of s. This quasi-vertical segment is located at an $O(1/\tau_\theta)$-distance of the Hopf point at s_{Hopf}, that is, near the canard value at $s_c \approx 0.95704$. Next, we explain how canard orbits are formed from the early stages of the canard explosion until the formation of the first spike, see Figure 3, as well as for the second and third spikes, see Figures 4.

In order to understand the canard trajectories structuring these periodic orbits, we need to examine the bifurcation diagram of the (a, d) fast subsystem with respect to θ for $s \approx s_c$. The θ-dependent family of equilibrium points $(a^*, d^*) = (a^*, d_\infty(a^*))$ of the fast subsystem is defined by

$$\{a_\infty(w\, d\, s\, a - \theta - \theta_0) - a = 0\} \cap \{d_\infty(a) - d = 0\}$$

that is

$$\left\{\theta = k_a \ln\left(\frac{1}{a} - 1\right) + w\, d_\infty(a)\, s\, a - \theta_0\right\}, \tag{7}$$

and forms a Z-shaped curve for $a \in (0, 1)$ (blue curve in Figure 2) with two fold points at $\theta_f^l = 0.18326$ and $\theta_f^r = 0.2432$. The lower branch consists of stable nodes for $\theta > \theta_f^l$. Saddle equilibria, whose invariant manifolds are weaker in the stable direction than in the unstable direction, lie along the middle branch between θ_f^l and θ_f^r. The upper branch has stable focuses until the supercritical Hopf bifurcation at $\theta_{Hopf} \approx 0.21335$, which gives a narrow paraboloid of limit cycles. This paraboloid folds back at $\theta_{Fold-cycle} \approx 0.21423$ towards the middle branch of saddles and makes a saddle-homoclinic connection at $\theta_{Homoclinic} \approx 0.21343$. The inner cycles, between θ_{Hopf} and $\theta_{Fold-cycle}$, are stable, while the outer cycles, between $\theta_{Fold-cycle}$ and $\theta_{Homoclinic}$, are unstable. The upper branch hosts unstable equilibria of focus type between θ_{Hopf} and $\theta \approx 0.241448$, then unstable nodes until θ_f^r. The bursting behaviour resulting from this bifurcation structure in the (a, d) fast subsystem is classified as a "Hopf/ fold cycle" bursting by Izhikevich [16].

After having dissected the (a, d) subsystem with respect to θ, we can focus on the slow-fast transitions in (6). Equation (7) defines the critical manifold $S^{0,(a,d,\theta)}$ of (6) where the only slow variable is θ. Therefore, the 1D slow flow lies along the folded set:

$$F^{(a,d,\theta)} = \left\{\frac{-k_a}{a(1-a)} + w\, s\, \left(a\, d'_\infty(a) + d_\infty(a)\right) = 0\right\}$$

with $d'_\infty(a) = \dfrac{d}{da}(d_\infty(a)) = -\dfrac{e^{(a-\theta_d)/k_d}}{k_d(1 + e^{(a-\theta_d)/k_d})^2}$. The critical points of $S^{0,(a,d,\theta)}$, i.e. the fold points, are at θ_f^l and θ_f^r. The passage of the slow nullcline $\{\theta = \theta_\infty(a)\}$ through the fold point θ_f^l in the 3D phase space as s varies slowly gives the transition from resting to spiking, then adds the spikes successively via canard trajectories until the bursting regime is reached.

The upper panels of Figure 3 show the first canard cycles induced by the Hopf bifurcation at s_{Hopf} in a similar analogy to that of the VDP-type planar systems: the trajectories move along the lower branch of stable nodes, pass through θ_f^l and follow 1D repelling slow manifolds before jumping to back to the branch of stable nodes (upper left panel in Figure 3). As s varies along the canard explosion, the canard cycles grow in amplitude up to the maximal canard while moving towards θ_f^r. These spikeless

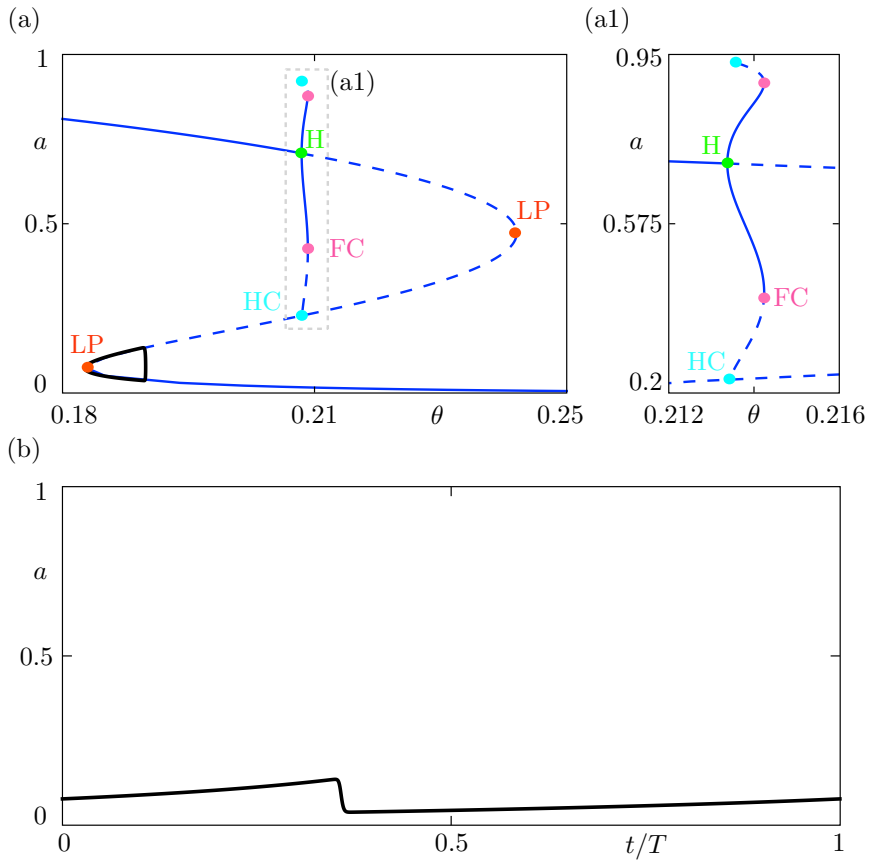

Figure 2: (a) Bifurcation diagram of the (a, d) fast subsystem upon variation of θ (blue), together with an example canard cycle of the (a, d, θ) system for $s \approx s_c$ (black). Panel (a1) corresponds to a zoom of panel (a) in the dashed rectangle. In both upper panels, H denotes a Hopf bifurcation, LP limit point bifurcations (folds) of equilibria, HC a Homoclinic bifurcation and FC a fold bifurcation of cycles. (b) Time series for variable a of the limit cycle shown in panel (a).

cycles are analogous to the canard without head trajectories in planar systems and the maximal canard is the excitability threshold of the (a, d, θ)-system.

When the limit cycle reaches to the right fold θ_f^r, the (un)stable manifolds of the equilibria shape the cycle. The invariant set of the saddle at θ_f^r expands the cycle in the a-direction, then brings it back towards the branch of the stable nodes. This expansion and contraction at θ_f^r gives birth to the first spike (the fourth trajectory in Figure 3). As s varies, the trajectory is repelled in the a-direction by the unstable manifolds of saddle points of the middle branch then attracted by the stable lower branch of $S^{0,(a,d,\theta)}$. This behaviour is similar to the canard with head cycles in the planar systems where a trajectory follows both attracting branches of the critical manifold. However, in the (a, d, θ)-system, the critical manifold contains repelling equilibria along the upper branch between θ_f^l and θ_{Hopf}. Thus, the trajectory returns to the lower branch once leaves the middle branch.

The formation of a cycle with one spike is completed once the spike is placed on the left of θ_{Hopf}. Note that it is still a canard cycle since a certain part of it lies along the unstable middle branch: it follows the stable branch as θ decreases towards θ_f^l, passes through the fold θ_f^l, continues along the unstable middle branch before departing in the direction of the unstable manifold towards the attracting focus. Since the (a, d) subsystem does not possess any cycle for $\theta < \theta_{Hopf}$ and the stable foci have weak attractions, the trajectory does not necessarily follow the upper branch of equilibria of the fast subsystem.

As s changes, the trajectory can follow again the 1D saddle-type slow manifold that stays close to the whole repelling branch of the critical manifold, provided it is exponentially close to it. This can only happen in the vicinity of the homoclinic bifurcation of the fast subsystem (for small enough $\varepsilon > 0$). Hence, as the trajectory comes close to the homoclinic point after the spike, it can grow a new canard segment and this initiates the formation of the next spike [15], see Figure 4. The second canard segment of the trajectory after the spike expands from $\theta_{Homoclinic}$ to θ_f^r: the limit cycle with one spike grows in the θ direction, gains the second spike at the right fold and then shrinks towards the left fold. Different than the first one, the second spike is aligned within the stable limit cycles of the (a, d) subsystem – which gives the fast oscillations of the burst episode. Note that the slow drift in θ may not allow the second spike to enter into the narrow paraboloid of the stable limit cycles (between θ_{Hopf} and $\theta_{Fold-cycle}$). As for the third (and later subsequent spikes), the family of stable cycles are drifted "inside the paraboloid" after passing through θ_{Hopf}, remain closer to the stable objects in that region (panel (18) of Figure 4). These fast oscillations terminate near $\theta_{Fold-cycle}$.

3 Folded node and MMOs in the (a, θ, s)-model

Tabak et al. have studied the effects of the cellular excitability and depression on the active and silent phases of episodic activity via the (a, θ, s)-model [35] which reads

$$\begin{aligned} \tau_a \dot{a} &= a_\infty(\tilde{w}\, s\, a - \theta - \theta_0) - a, \\ \dot{\theta} &= \varepsilon(\theta_\infty(a) - \theta), \\ \dot{s} &= \varepsilon\tilde{\tau}_s(s_\infty(a) - s), \end{aligned} \tag{8}$$

where $\tilde{\tau}_s = \tau_\theta/\tau_s$. The (a, θ, s)-model does not account for the fast kinetics of the activity-dependent depression, thus its network connectivity, $\tilde{w}$, takes different values than w of the (a, d, θ, s)-model. (We use $\tilde{w}$ in the following calculations but the dynamics remain qualitatively the same with a quasi-steady state approximation $d = d_\infty(a)$ ($\tilde{w} \approx w d_\infty(a)$).) The number of slow variables determines the dimension of the critical manifold and, hence, that of the slow flow on it. With the usual parameter set ($\tau_a = 1, \tau_\theta = 1000, \tilde{\tau}_s = \tau_\theta/\tau_s = 2$), the (a, θ, s)-model has one fast (a) and two slow variables (s, θ), therefore the a-nullsurface in (8) defines the critical manifold:

$$\begin{aligned} S^{0,(a,\theta,s)} &:= \{a_\infty(\tilde{w}\, s\, a - \theta - \theta_0) - a = 0\} \\ &:= \left\{ k_a \ln\left(\frac{1}{a} - 1\right) + \tilde{w} s a - \theta - \theta_0 = 0 \right\}. \end{aligned} \tag{9}$$

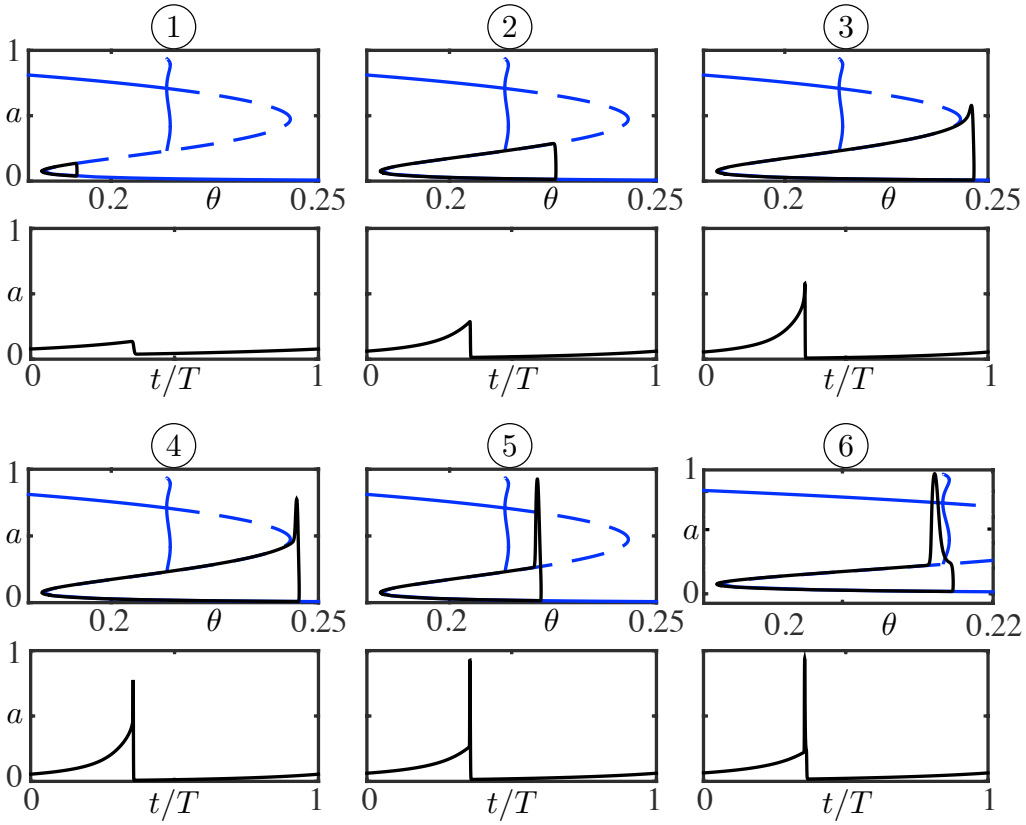

Figure 3: Formation of the first spike in system (6) upon exponentially small variation of $s \approx s_c$. Each up-down pair shows a solution superimposed on the bifurcation diagram of the (a, d) fast subsystem versus θ (upper panel) and the time course of the solution for variable a (lower panel). Panel (6) displays a zoomed view so as to better visualize the interaction between the spike and the bifurcation diagram of the fast subsystem.

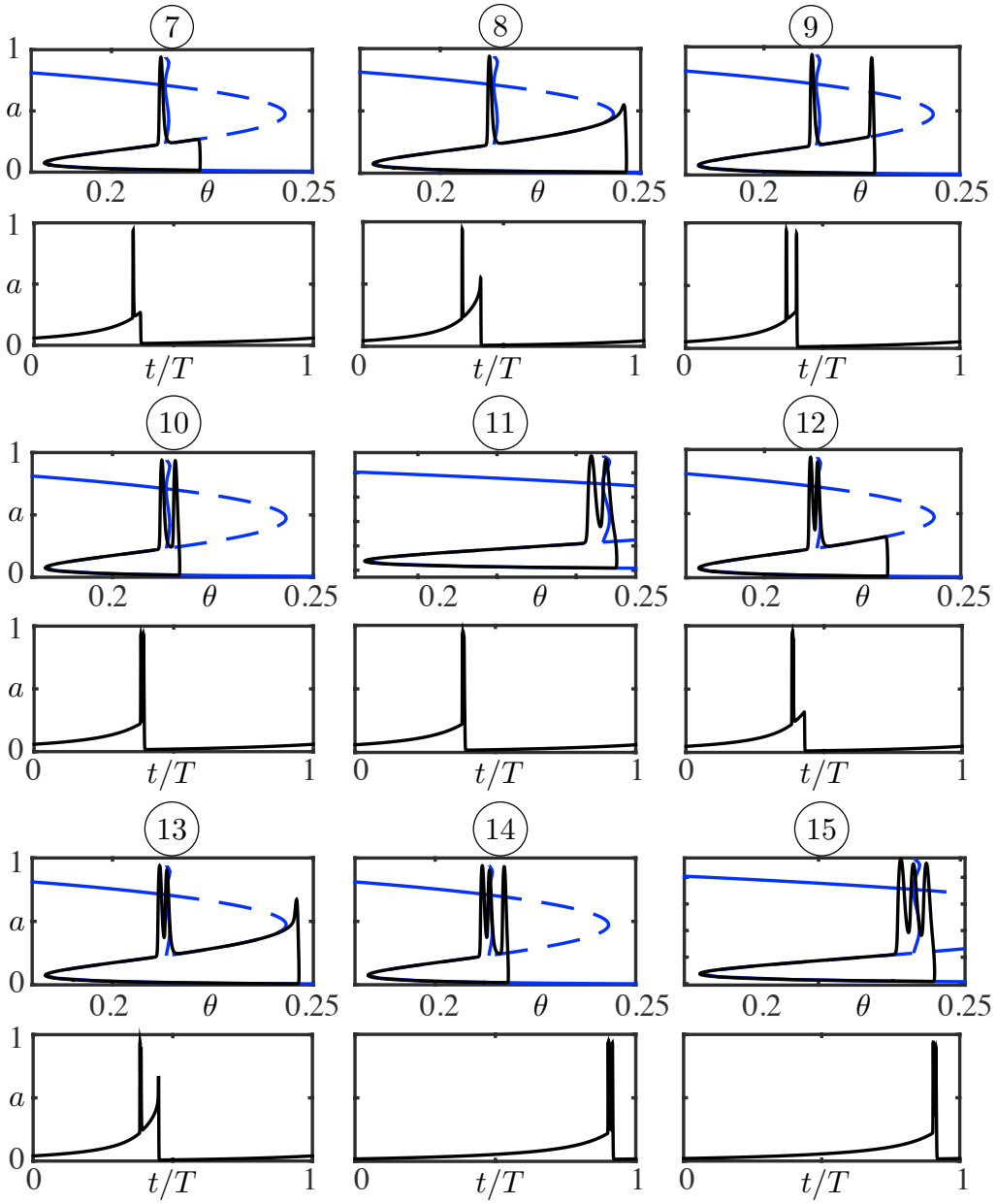

Figure 4: Formation of the second (panels (7) -(11)) and third (panels (12) -(15)) spikes in system (6) upon exponentially small variations of $s \approx s_c$. Each up-down pair shows a solution superimposed on the bifurcation diagram of the (a, d) fast subsystem versus θ (upper panel) and the time course of the solution for variable a (lower panel). Panels (11) and (15) display zoomed views so as to better visualize the interaction between the spikes and the bifurcation diagram of the fast subsystem.

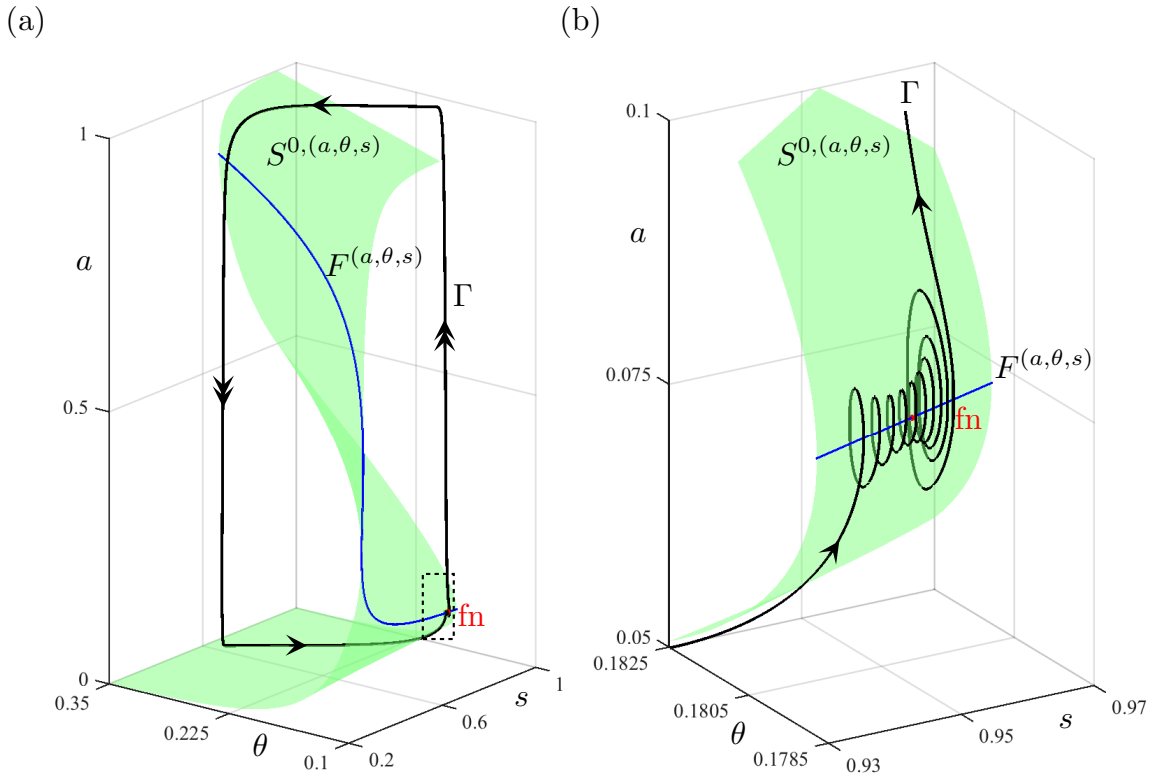

Figure 5: (a) MMO solution Γ of system (8) for $\tilde{w} = 0.7625$; also shown are the critical manifold $S^{0,(a,\theta,s)}$, the fold curve $F^{(a,\theta,s)}$ (blue) and the folded node fn (red dot). (b) zoom near the folded node (dashed rectangle in panel (a)).

Figure 5 shows $S^{0,(a,\theta,s)}$ with the fold curve (blue), that is

$$F^{(a,\theta,s)} = \left\{ \frac{-k_a}{a(1-a)} + \tilde{w}s = 0 \right\}.$$

The black curve shown in Figure 5 is an example MMO-type periodic orbit of (8). As we have mentioned in the introduction, the SAOs of MMOs appear due to the presence of folded singularities on the fold curve, in particular near a folded node. Below we investigate the limiting slow dynamics near $F^{(a,\theta,s)}$ using the DRS approach described in the introduction. The first step is to set the smallest timescale parameter $\varepsilon = 1/\tau_\theta$ to zero in the fast-time parametrisation of system (8), and obtain the following differential-algebraic problem:

$$\begin{aligned} 0 =& a_\infty(\tilde{w}sa - \theta_0 - \theta) - a, \\ \dot{\theta} =& \theta_\infty(a) - \theta, \\ \dot{s} =& \tilde{\tau}_s(s_\infty(a) - s). \end{aligned} \tag{10}$$

The algebraic condition in (10) defines the critical manifold $S^{0,(a,\theta,s)}$ given in (9). Differentiating $S^{0,(a,\theta,s)}$ with respect to time, and projecting onto the (a,s)-space leads to the following system of differential equations:

$$\begin{aligned} -\left(\frac{-k_a}{a(1-a)} + \tilde{w}s\right)\dot{a} &= -\dot{\theta} + \tilde{w}a\dot{s} = -(\theta_\infty(a) - \theta) + \tilde{w}a\tilde{\tau}_s(s_\infty(a) - s) \\ \dot{s} &= \tilde{\tau}_s(s_\infty(a) - s), \end{aligned} \tag{11}$$

with θ constrained to be on $S^{0,(a,\theta,s)}$, that is

$$\theta = k_a \ln\left(\frac{1}{a} - 1\right) + \tilde{w}sa - \theta_0 = \theta(a,s).$$

The singularities of equation (11) along the fold curve $F^{(a,\theta,s)}$ can be overcome through desingularization by applying a time rescaling of factor $\frac{k_a}{a(1-a)} - \tilde{w}s$, which gives the DRS:

$$\begin{aligned} a' &= -\theta_\infty(a) + \theta(a,s) + \tilde{w}a\tilde{\tau}_s(s_\infty(a) - s), \\ s' &= \left(\frac{k_a}{a(1-a)} - \tilde{w}s\right)\tilde{\tau}_s(s_\infty(a) - s). \end{aligned} \tag{12}$$

Note that desingularization reverses the direction of flow on the repelling sheet of $S^{0,(a,\theta,s)}$ where $\frac{k_a}{a(1-a)} - \tilde{w}s < 0$. Hence, the phase portrait of the reduced system is obtained by changing the direction of the flow in the phase portrait of the DRS where for $\frac{k_a}{a(1-a)} - \tilde{w}s < 0$.

The structure of (12) does not allow symbolic calculation of the equilibria, but the computed bifurcation diagram with respect to $\tilde{w}$ shows the properties of its equilibria (Figure 6-(a)). Black and red branches of equilibria, one being stable the other unstable, exchange stability through a transcritical bifurcation at $\tilde{w}_T \approx 0.754645$. For $\tilde{w} < \tilde{w}_T$, the nodes of (12) are the true equilibria of (8) and the saddles are folded saddles. The solutions of (8) for $\tilde{w} < \tilde{w}_T$ are not affected by the folded saddles in this region because trajectories of (8) are attracted by the node equilibria. On the other hand, the nodes of (12) become folded nodes when $\tilde{w} > \tilde{w}_T$ because they are on $F^{(a,\theta,s)}$ (example phase portrait in Figure 6-(b)), while the saddles on the $s = s_\infty(a)$ curve turn into saddle-foci of the 3D system, with complex eigenvalues with positive real parts and one negative real eigenvalue. The presence of these two close equilibria (falls into the *folded saddle-node type II* [34]) is the footprint of the mechanism responsible for the small subthreshold oscillations: for big enough time-scale difference between the fast and slow components of the system, the orbits approach the folded node, around which there is as funnel structure that first attracts the orbits with a inward spiralling motion, and then repels them towards the 2D invariant manifold of the saddle of the full 3D system. Finally, the 2D unstable manifold of the saddle (associated with its the complex eigenvalues) provokes additional small oscillations just before the orbit leaves the vicinity of the critical manifold.

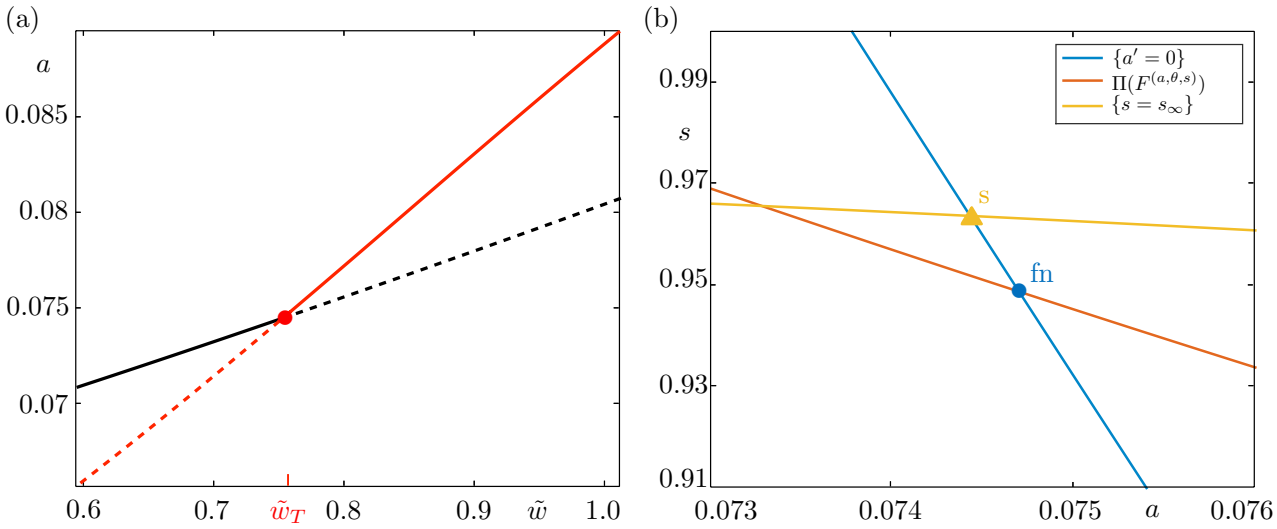

Figure 6: (a) Bifurcation diagram of (12) with respect to $\tilde{w}$. Solid (resp. dashed) lines correspond to stable (resp. unstable) equilibria, and both branches cross at $\tilde{w}_T = 0.754645$, where they exchange stability via a transcritical bifurcation (marked by a red dot); note that the branch plotted in red corresponds to the projection of the fold curve onto the (a, s)-plane. (b) Phase portrait of (12) for $\tilde{w} = 0.7625$. The node equilibrium corresponds to a folded node fn for the reduced system, with coordinates $(a_{\text{fn}}, s_{\text{fn}}) \approx (0.074696, 0.94875)$; it lies at the intersection between the a-nullcline (blue) and the projection $\Pi(F^{(a,\theta,s)})$ of the fold curve onto the (a, s)-plane (red). The saddle equilibrium s, with coordinates $(a_{\text{s}}, s_{\text{s}}) \approx (0.074426, 0.96368)$, lies at the intersection between the a-nullcline (blue) and the $\{s = s_\infty\}$-component of the s-nullcline (yellow).

3.1 MMOs and behaviour along isolas

Figure 7-(a) shows the bifurcation diagram the (a, θ, s)-model. The system undergoes a supercritical Hopf bifurcation at $\tilde{w}_{Hopf} \approx 0.755319$. The periodic solutions lie along the red branch starting at $\tilde{w}_{Hopf}$ grow in amplitude until $a_{max} = 1$, which are the relaxation type solutions studied in [35] (Figure 8-(b)).

The periodic solutions along the Hopf branch are unstable between two period doubling (PD) bifurcations at $\tilde{w} \approx 0.758948$ and $\tilde{w} \approx 0.771919$. These unstable solutions are canard orbits that follow the unstable middle surface of $S^{0,(a,\theta,s)}$. The stable solutions between $\tilde{w} \approx [0.758948, 0.771919]$ are MMO-type periodic orbits: n-number of SAOs near the folded node of $S^{0,(a,\theta,s)}$ followed by a LAO of relaxation type (Figure 5-(a)). All solutions with the same number of SAOs belong to the same isolated closed curve of periodic orbits, a so-called *isola*. Stable solutions lie on the top of each isola between two PD bifurcations on each. It is possible to pass from one isola to the next as $\tilde{w}$ changes within the approximate interval $[0.758948, 0.771919]$. Transitions between neighbouring isolas corresponds to a ± 1 change in the number of SAOs. The time course of some of these periodic orbits are given in Figure 8-(a).

The 9-SAO isola is displayed in Figure 7-(b) as an example. Observe that, similar, to the quasi-vertical segments (already mentioned earlier as a trademark of canard explosion) that one encounters in the s-bifurcation diagram for the (a, d, θ)-model, the isolas present two high-slope segments between the bottom right corner (points 2 and 11) and the plateau on the top (see points 6 and 8 in the inset plot). We keep referring to them as the *quasi-vertical segments* of the solution branches. They connect the small-amplitude orbits to MMO-type orbits via canard explosions. Example periodic orbits on the left and right quasi-vertical segments are given in Figures 9 and 10, respectively. The orbit at the bottom left of the isola is in Figure 9-(1). This subthreshold orbit has the shortest segment along the repelling surface and it has 9 SAOs plus one last oscillation slightly larger than the others. When moving $\tilde{w}$ on the left quasi-vertical segment, the associated cycle extends the part of its last oscillation along the repelling middle sheet of $S^{0,(a,\theta,s)}$ (the orbits on panels (1)-(3) are similar to the canard-without-head cycles in planar systems). The maximal canard trajectory is the solution that stretches out between

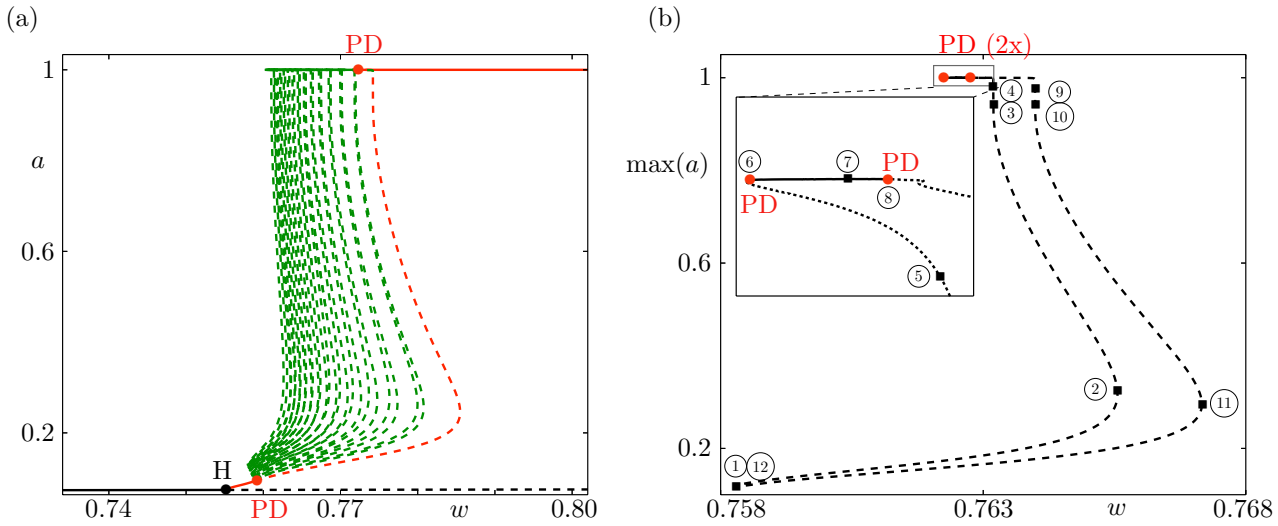

Figure 7: (a) Bifurcation diagram of the (a, θ, s)-model with isolas of MMO solutions. (b) Zoom of panel (a) near the 9-SAO-isola. The inset panel offers a further zoom into the upper region the isola. Bold lines correspond to stable solutions, dashed lines represent unstable ones. In all panels, red (resp. black) dots indicate period-doubling (resp. Hopf) bifurcations. In panel (b) and its inset, marked solutions are shown in Figures 9 and 10.

two folds (the fourth orbit). As $\tilde{w}$ changes, the solution follows the upper attracting sheet of the critical manifold, then jumps back to repelling sheet, finally funnels into the folded-node region (the last two orbits are similar to the canard-with-head cycles in planar systems). The formation of the relaxation segment of the period solution (the LAO) is completed when $\tilde{w}$ passes the first PD bifurcation point (Figure 9-(6)), where the solutions become stable.

As $\tilde{w}$ continues to move along the isola, periodic orbits lose their stability at the second PD point, then they shrink in amplitude while the parameter goes down along the right quasi-vertical segment. Here we observe a second canard explosion, which happens in the opposite direction as the usual one (in a sense, a canard *implosion*), connecting the MMOs to the small-amplitude periodic orbits (Figure 10). We see that the only difference between the solutions on the left and right quasi-vertical segments is the amplitude of the 9th SAO, which is slightly larger than the ones along the left quasi-vertical segment.

The bifurcation structure of this model, in particular the family of isolas of MMOs, their shape and organization in parameter space, is very much exemplary of excitable systems with one fast and two slow variables near a folded node. Indeed, such bifurcation structure has been found in various single neuron models (e.g. in the reduced Hodgkin-Huxley model) and also in models of chemical reactions such as the Koper model; see [8] for details and further examples.

4 Canard-mediated MMBOs oscillations in the (a, d, θ, s)-model

In Section 2 we tracked the s-dependent family of canard cycles in the (a, d, θ) burster. In Section 3, we detailed the MMO behaviour formed by an alternation between canard-mediated subthreshold oscillations and one LAO in the (a, θ, s)-model. In this section, we combine the bursts with MMOs in the 4D system (4), and focus on the canard trajectories of the resulting MMBOs. We consider the network connectivity parameter, w, as the main bifurcation parameter of (4), while other parameters are chosen as in [37]. This is a quite reasonable assumption since the model represents a developmental process where the network connectivity changes.

We start by investigating the slow flow near the critical manifold (4). The critical manifold is a surface

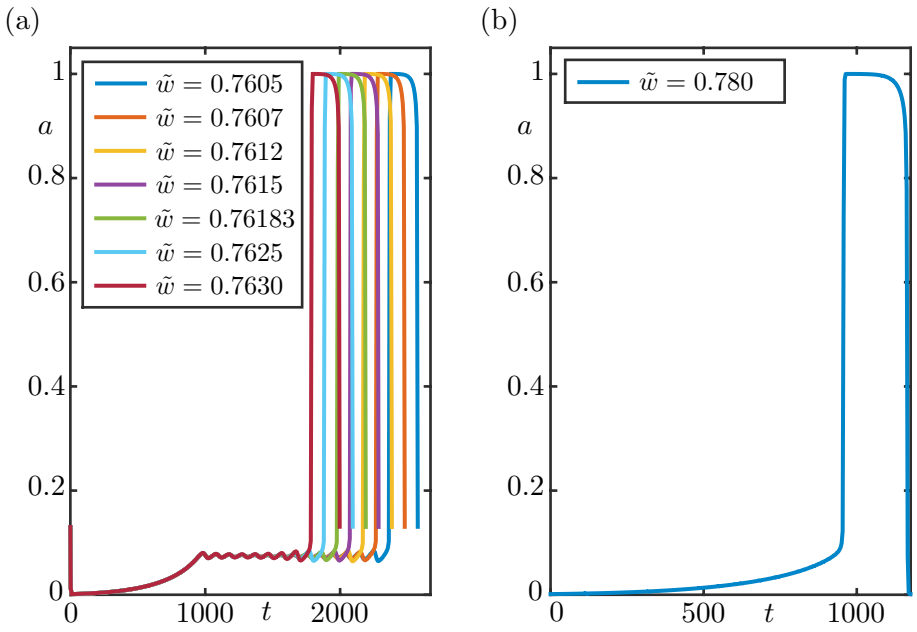

Figure 8: (a) Example MMO-type solutions of the (a, θ, s)-model for $\tilde{w} \in [0.758948, 0.771919]$. (b) A relaxation-type solution of the (a, θ, s)-model for $\tilde{w} = 0.78$.

in $\mathbb{R}^4$, defined by the algebraic equation:

$$\begin{aligned} S^0 &:= \{a_\infty(w\, d\, s\, a - \theta - \theta_0) - a = 0,\ d_\infty(a) - d = 0\} \\ &:= \left\{ k_a \ln\left(\frac{1-a}{a}\right) + w\, d_\infty(a)\, s\, a - \theta - \theta_0 = 0 \right\}. \end{aligned} \tag{13}$$

Since two slow variables, θ and s, appear in the expression of S^0, the slow flow is 2D on the critical surface. The critical manifold S^0 is folded along the folded curve F:

$$F = \left\{ \frac{-k_a}{a(1-a)} + w\, s\, \left(a\, d'_\infty(a) + d_\infty(a)\right) = 0 \right\}.$$

Keeping θ on S^0 by setting $\theta = -\theta_0 + k_a \ln\left(\frac{1-a}{a}\right) + w\, s\, a\, d_\infty(a)$, the DRS is given by

$$\begin{aligned} a' &= -\left(\theta_\infty(a) - \left(-\theta_0 + k_a \ln(\frac{1-a}{a}) + w\, s\, a\, d_\infty(a)\right)\right) + \tilde{\tau}_s w\, a\, d_\infty(a)\, (s_\infty(a) - s)\,, \\ s' &= -\left(\frac{-k_a}{a(1-a)} + ws\, \left(a\, d'_\infty(a) + d_\infty(a)\right)\right) \tilde{\tau}_s\, (s_\infty(a) - s)\,. \end{aligned} \tag{14}$$

Note that since the dynamics of d can be expressed as a function of a in (13), i.e. $d = d_\infty(a)$, the most general way to derive DRS given in (3) is not necessary. The bifurcation diagram of (14) with respect to w is presented in Figure 11-(a). Similar to the one of (12), two sets of equilibria of saddle- and node-types (red and black curves) undergo a transcritical bifurcation at $w_T \approx 1.4218$ (a folded saddle-node type II event). For $w > w_T$, the nodes of the DRS, (a_f, s_f), lie on the folded curve F and correspond to folded-node singularities of (4) (see an example of phase portrait on Figure 11-(b)). On the other hand, the saddle-type equilibria, (a_s, s_s) satisfy $s = s_\infty(a)$, thus they are also equilibria of the full system (4). In this region of parameter space (i.e. $w > w_T$) and for small enough values of the timescale separation parameter ε, then the MMO trajectories of (4) can be trapped by the funnel surrounding the folded node. They first make SAOs inside the funnel towards the folded node, pass near it and then are likely to continue displaying SAOs close to the repelling side of S^0 along the 1D attracting manifold of the saddle equilibrium of the full system, before being repelled by spiralling away along the 2D unstable manifold of the saddle. This 2D unstable manifold associated with the complex eigenvalues of the saddle hence provokes additional small oscillations just before the orbit leaves the vicinity of the critical manifold and enters into the burst phase. Note that resulting periodic orbits with SAOs and bursting oscillations, that is MMBOs, are possible in system with at least 2 fast and 2 slow variables.

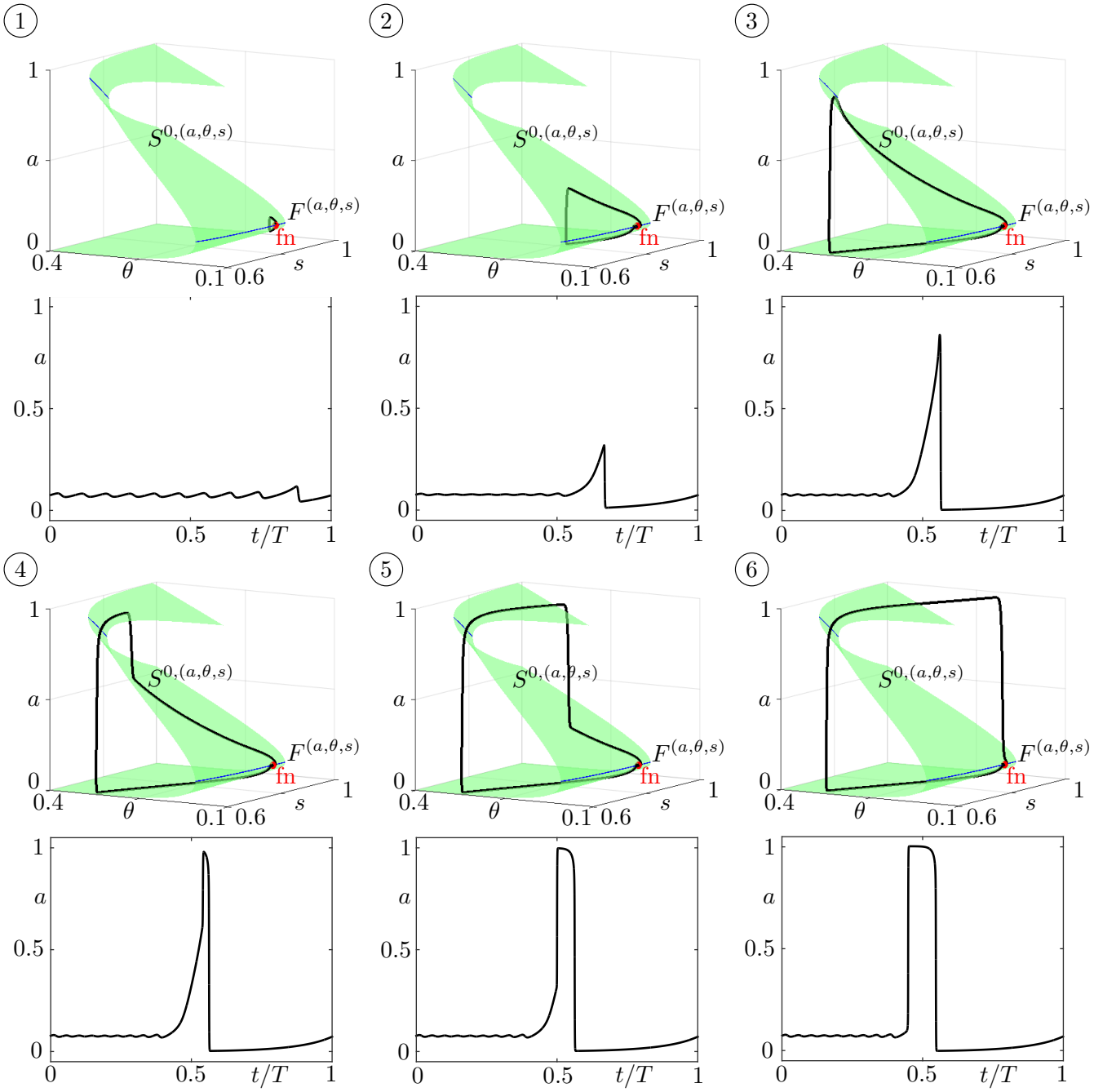

Figure 9: Upward behaviour of the orbits when w moves along the left quasi-vertical segment of the isola on panel (b) of Figure 7. A canard explosion connects in parameter space a SAO periodic orbit (upper left) to a MMO periodic orbit (bottom right). The green surface is the critical manifold $S^{0,(a,\theta,s)}$, the blue lines on $S^{0,(a,\theta,s)}$ correspond to the single fold curve $S^{0,(a,\theta,s)}$ (the critical manifold is in fact a cusp surface). Each panel below the (a,θ,s)-space projection shows the time course for a of the periodic orbit shown above.

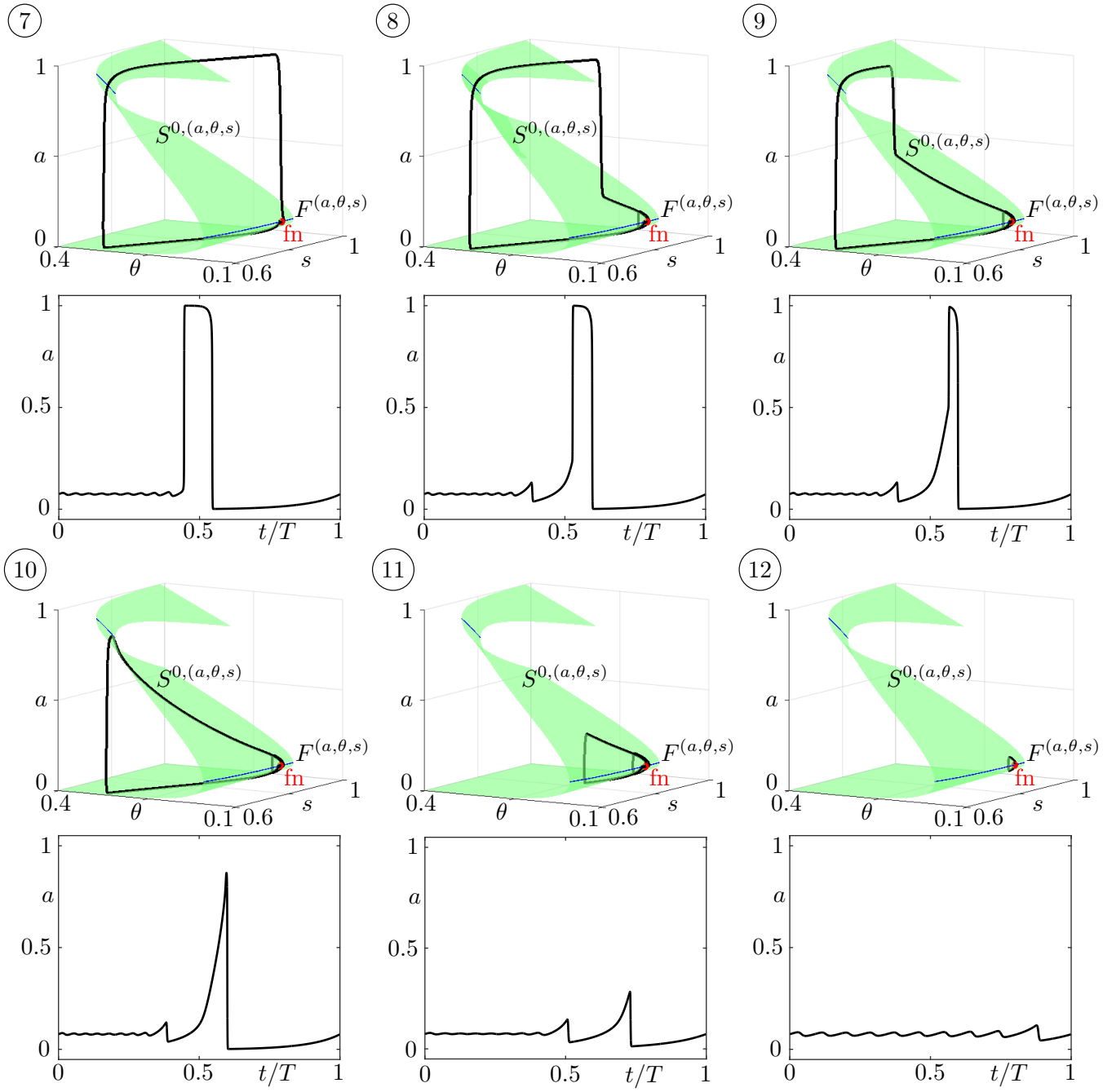

Figure 10: Downward behaviour of the orbits when w moves along the right quasi-vertical segment of the isola on panel (b) of Figure 7. A canard implosion connects in parameter space the MMO periodic orbit (upper left) to SAO periodic orbit (bottom right). The green surface is the critical manifold $S^{0,(a,\theta,s)}$, the blue lines on $S^{0,(a,\theta,s)}$ correspond to the single fold curve $S^{0,(a,\theta,s)}$ (the critical manifold is in fact a cusp surface). Each panel below the (a,θ,s)-space projection shows the time course for a of the periodic orbit shown above.

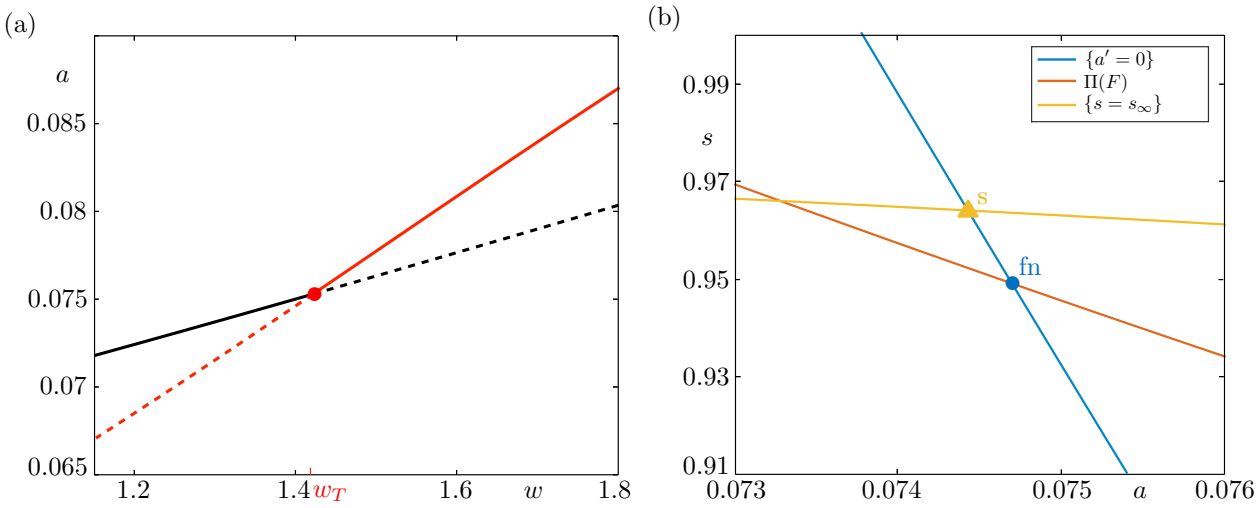

Figure 11: (a) Bifurcation diagram of (14) with respect to w. Solid (resp. dashed) lines correspond to stable (resp. unstable) equilibria, and both branches cross at $w_T = 1.4218$, where they exchange stability via a transcritical bifurcation; note that the branch plotted in red corresponds to the projection of the fold curve onto the (a, s)-plane. (b) Nullclines of (14) for $w = 1.43$: in blue, the a-nullcline; in red and yellow, both components of the s-nullcline. Also shown are the two equilibria of the system: the saddle equilibrium s with coordinates $(a_s, s_s) \approx (0.0753962, 0.962052)$ lies at the intersection between the a-nullcline (blue) and the $\{s = s_\infty\}$-component of the s-nullcline (yellow); the folded-node fn with coordinates $(a_{\text{fn}}, s_{\text{fn}}) \approx (0.0755447, 0.954177)$, lies at the intersection between the a-nullcline (blue) and the projection $\Pi(F)$ of the fold curve onto the (a, s)-plane (red).

4.1 MMBOs and behaviour along isolas

Figure 12 shows the bifurcation diagram of the (a, d, θ, s)-model with respect to parameter w. At $w_H \approx 1.42122$ the system undergoes a supercritical Hopf bifurcation, where a branch of periodic solutions of bursting type arises (Figure 13-(b)). Periodic solutions along this branch are unstable between two PD bifurcations at $w \approx 1.43103$ and $w \approx 1.47011$. The stable solutions of the system between these two PD bifurcations are the MMBO-type orbits that reside on isolas in $w \approx [1.42748, 1.47011]$ (see example solutions in Figure 13-(a)). The transcritical bifurcation of (14) at $w_T \approx 1.4218$ can be considered as a lower bound for MMBO dynamics as $\varepsilon \to 0$. The isolas are more densely positioned for w-values closer to w_H. The last isola overlaps with the branch of the bursting-type solutions (blue curve superimposed on the red branch arising at the Hopf point). Each isola corresponds to a particular sector of rotation of canard solutions near the folded node yielding SAOs, and each periodic orbit with n-SAOs lies on a different isola. A variation of $w \in [1.42748, 1.47011]$ can move an orbit from one sector to another and, consequently, change the number of SAOs of the solution (Figure 13-(a)). We show a representative selection of the family of isolas but there may be more of them. Given that each isola can be associated with a given number of SAOs, one can obtain a prediction of the number of isolas by computing the maximal rotation number given by the ratio of the eigenvalues of the folded node (as a node equilibrium of the DRS); see [8] for details. This is only a prediction valid for small-enough $\varepsilon > 0$. This number, and hence the number of isolas, will increase up to infinity as the folded node approaches a folded saddle-node transition. In the present work, we do not to expand on these questions.

Figure 14 shows the isola formed by the 18-SAO-orbits. Along the isola, canard trajectories organise the transition from the "pure" subthreshold SAO-solutions to spiking, and then to MMBO-type solutions (similar to the spike-adding canard explosion in the (a, d, θ)-model). The orbit in Figure 15-(1) has 18 SAOs plus one last SAO containing a canard segment with larger amplitude. As w varies following the left branch of the isola, that canard segment expands along the middle sheet of S^0. It grows until the upper fold of S^0 and becomes a maximal canard segment (which approximates the spiking threshold) of the left branch of the isola (Figure 15-(3)). When the orbit reaches the upper

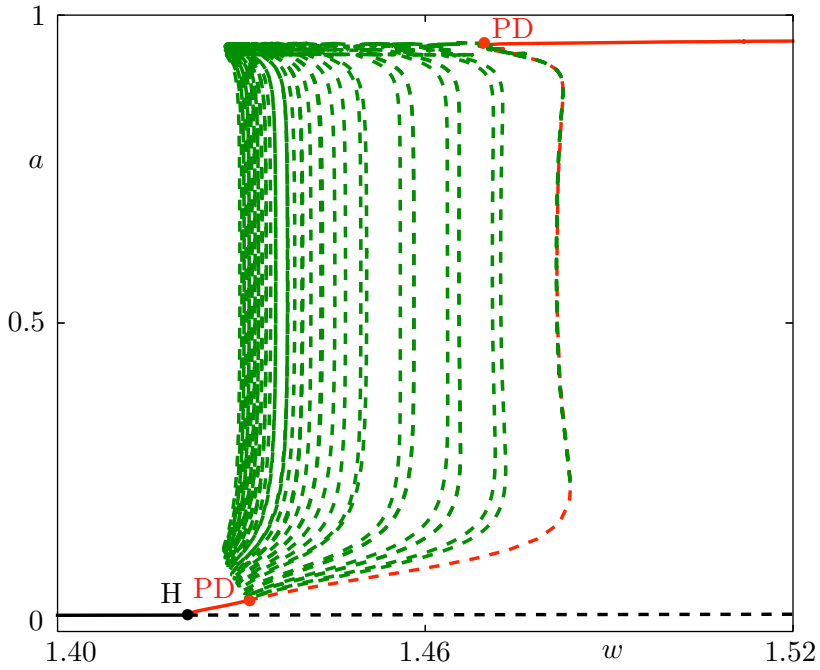

Figure 12: Bifurcation diagram of the (a, d, θ, s)-model with isolas of the MMBO solutions; solid lines correspond to stable solutions, dashed lines to unstable ones. Red dots indicate PD bifurcations and the black dot corresponds to the Hopf bifurcation. The branch of equilibria (black) undergoes a Hopf bifurcation at w_H, which gives rise to a branch of periodic solutions (red) which is unstable between the PD bifurcations at $w_{D1} \approx 1.42748$ and $w_{D2} \approx 1.47011$. Isolas of MMBO-type periodic oscillations are shown in green.

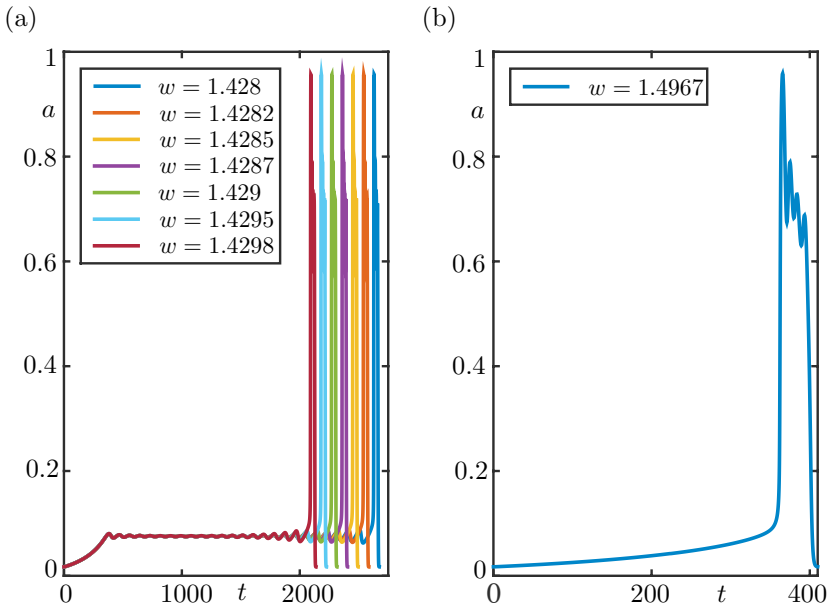

Figure 13: (a) Example of MMBO-type solutions of the (a, d, θ, s)-model for w in the approximate interval $[1.428, 1.47]$. Each solution corresponds to particular isola from Figure 12. (b) Bursting behaviour (without SAOs) of the (a, d, θ, s)-model for $w = 1.4967$.

fold of S^0, the stable and unstable manifold of the associated slow manifold expand and contract it in the a-direction. Finally the orbit crosses the middle branch (the spiking threshold [36]) and the first spike appears Figure 15-(4)). As w decreases, the canard segment shrinks while the formation of the spike continues. The solution with a fully formed spike has 18 SAOs and 1 LAO (Figure 15-(6)) and it lies on the left corner of the quasi-horizontal branch of the isola that has a sharp fold at $a_{max} \approx 0.94$ (Figure 14-(b)).

As w changes, the orbits move leftwards along the lower branch emanating form the sharp turning point at $a_{max} \approx 0.94$ and the second canard segment, which is located after the spike, expands; see orbits (6) to (8) on Figure 14-(b). The solution with one spike and the longest canard segment corresponds to orbit (8) and just after, a new spike appears. As we move along the upper fold, the canard segment between two spikes shrinks. The solution becomes a periodic orbit with 18 SAOs and 2 spikes when it reaches the left fold point of the second quasi-horizontal segment of the branch around $a_{max} \approx 0.948$ ((9) on Figure 14-(b)). The third and fourth spikes are formed through the same principles: orbits lose spikes as w varies towards the bottom of the isola along its right branch – similar to the canard implosion described in Section 3.

The period of a canard cycle is closely related to the length of its repelling segment [7, 18]. Along a canard explosion in a planar VDP-type system, the period function is increasing between the Hopf bifurcation and the maximal canard cycle, and it is decreasing from the maximal canard to the relaxation regime. Thus the maximal canard cycle, being the solution with the longest repelling segment, has the longest period [7]. This property holds in MMBOs as well. Figure 14-(c) shows the period plotted against w along one of the isolas just described; it clearly has a complex leaf-structure with multiple local maxima. The behaviour of the period along each leaf resembles a "local" canard explosion: orbits on each local maximum (orbits 3, 8, 11, 14) correspond to maximal canard solutions of each leaf, and the orbits (1, 6, 9, 12, 15) on local minima have the shortest canard segments. Among these solutions, Orbit (1) corresponds to the global minimum of the isola, therefore it the "fastest" solution with 18 SAOs.

5 Conclusion

We have revisited a group of related rate models introduced and analysed in [37, 36, 35] from the viewpoint of multiple-timescale dynamics and complex oscillations. The complete system contains 4 variables (2 fast and 2 slow), where the fast subsystem corresponds to a recurrent excitatory network with fast activity-dependent synaptic depression, which can produce oscillations [37]. In this work, we have considered three different combinations of the 4 variables and analysed them using notions from geometric singular perturbation theory (GSPT). In particular, we have focused on the excitable structure of each model in link with canard solutions. Adding either the dynamics of the cell firing threshold ((a, d, θ) model) or long-term synaptic depression ((a, d, s) model), bursting oscillations are generated [37]; we have described them through their canard-mediated spike-adding structure.

We have also investigated the combined effect of the threshold for cell firing and the long-term synaptic depression on the network activity by studying the slow flow associated to the (a, θ, s) model, which turns out to display canard-induced MMOs due to the presence of a folded-node singularity. Moreover, we have been able to understand the structure of families of MMOs organised in parameter space along isolas, as one typically expects from such slow-fast systems.

Finally, we have gathered all four variables in the complete (a, d, θ, s) model, which displays complex oscillations that can be described as a mix between MMOs and bursting. These fall into the category of MMBOs introduced in [9]. We computed for the first time the remarkable bifurcation structure of MMBOs, also organised in families of isolas that retain the salient features of both the isolas of MMOs and of bursting oscillations from the associated aforementioned 3D systems. In each case, isolas can be understood as a way for the system to single-out specific oscillatory patterns.

One noticeable aspect of MMBO solutions is the presence of SAOs in between bursts. In relation to some experimental data shown in the papers by O'Donovan et al. and on which the network activity comprises fluctuations below threshold, we advocate for the MMBO framework as an alternative to simply noise in order to account for these experimentally-observed subthreshold fluctuations. The

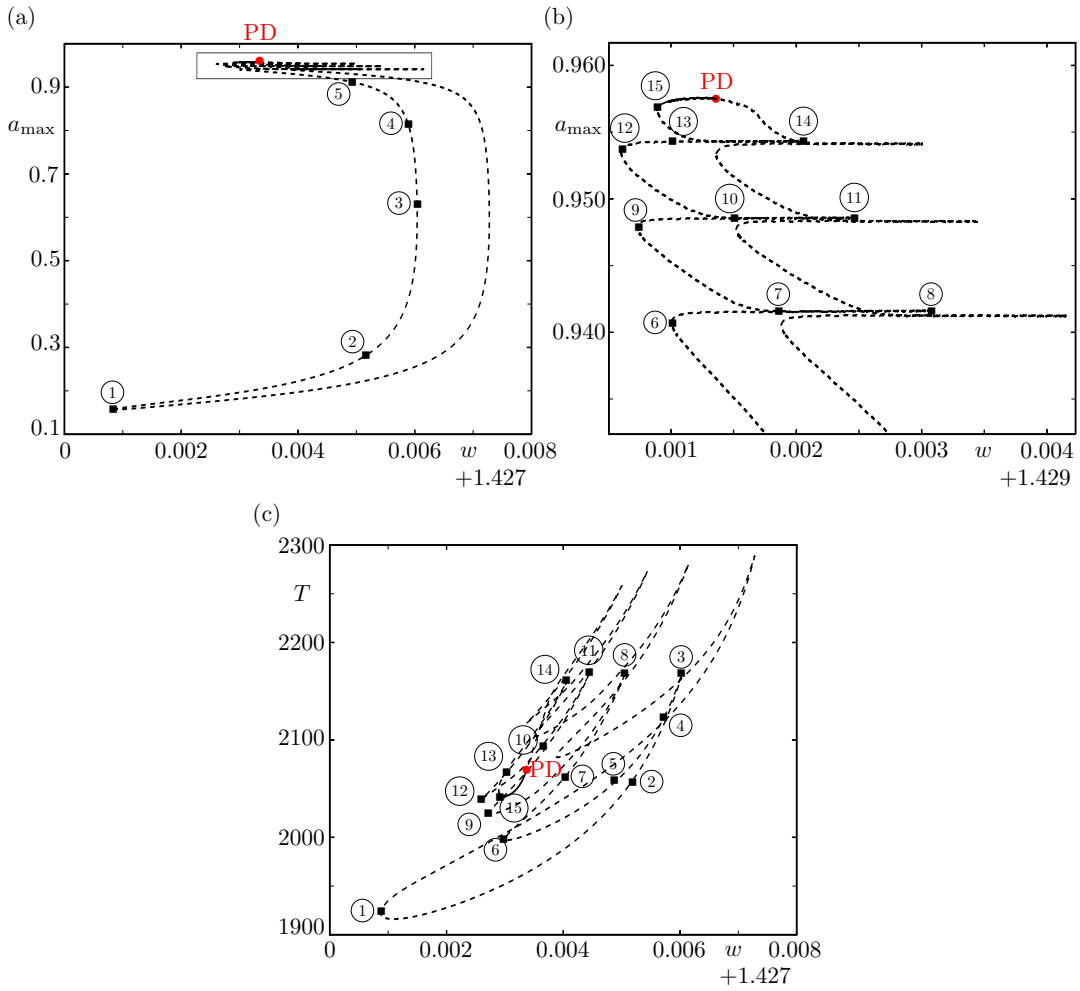

Figure 14: (a) The isola corresponding to MMBO orbits with 18 SAOs. (b) Zoom into the upper branch of the isola highlighted as an inset in panel (a). (c) Period along the isola shown in panel (a). The profile of the solutions marked by a black square are shown in Figures 15-16. In all panels, solid curves correspond to stable solutions while dashed curves correspond to unstable solutions.

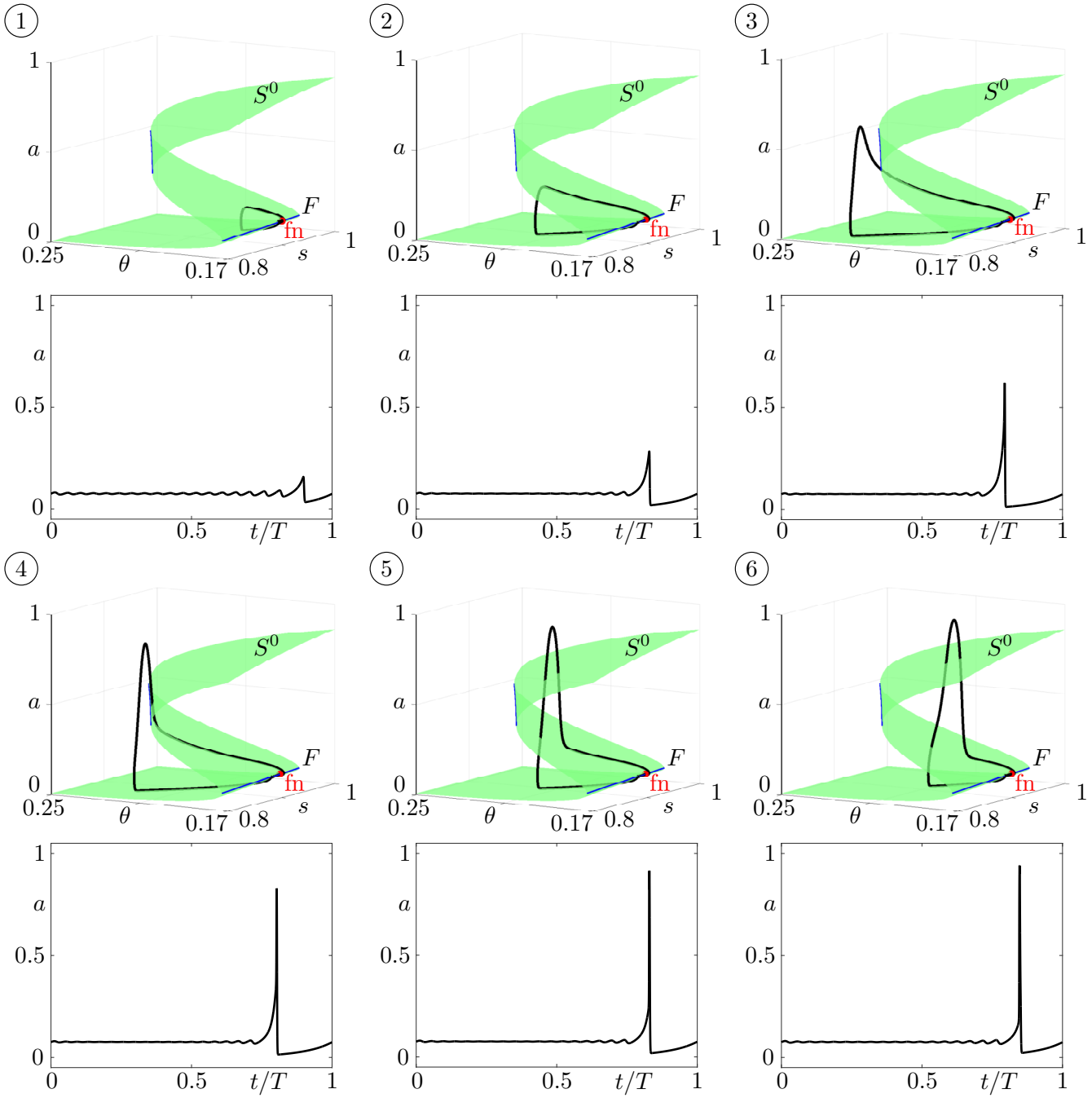

Figure 15: Birth of the first canard-mediated spike along the isola corresponding to MMBO solutions with 18 SAOs in Figure 14 as w varies. Each up-down pair shows the solution projected onto the (θ, s, a)-space (upper panel) and the a-time course of the solution (lower panel). The green surface is the critical manifold S^0 and the blue curve is the lower fold F, the red dot marks the folded node fn.

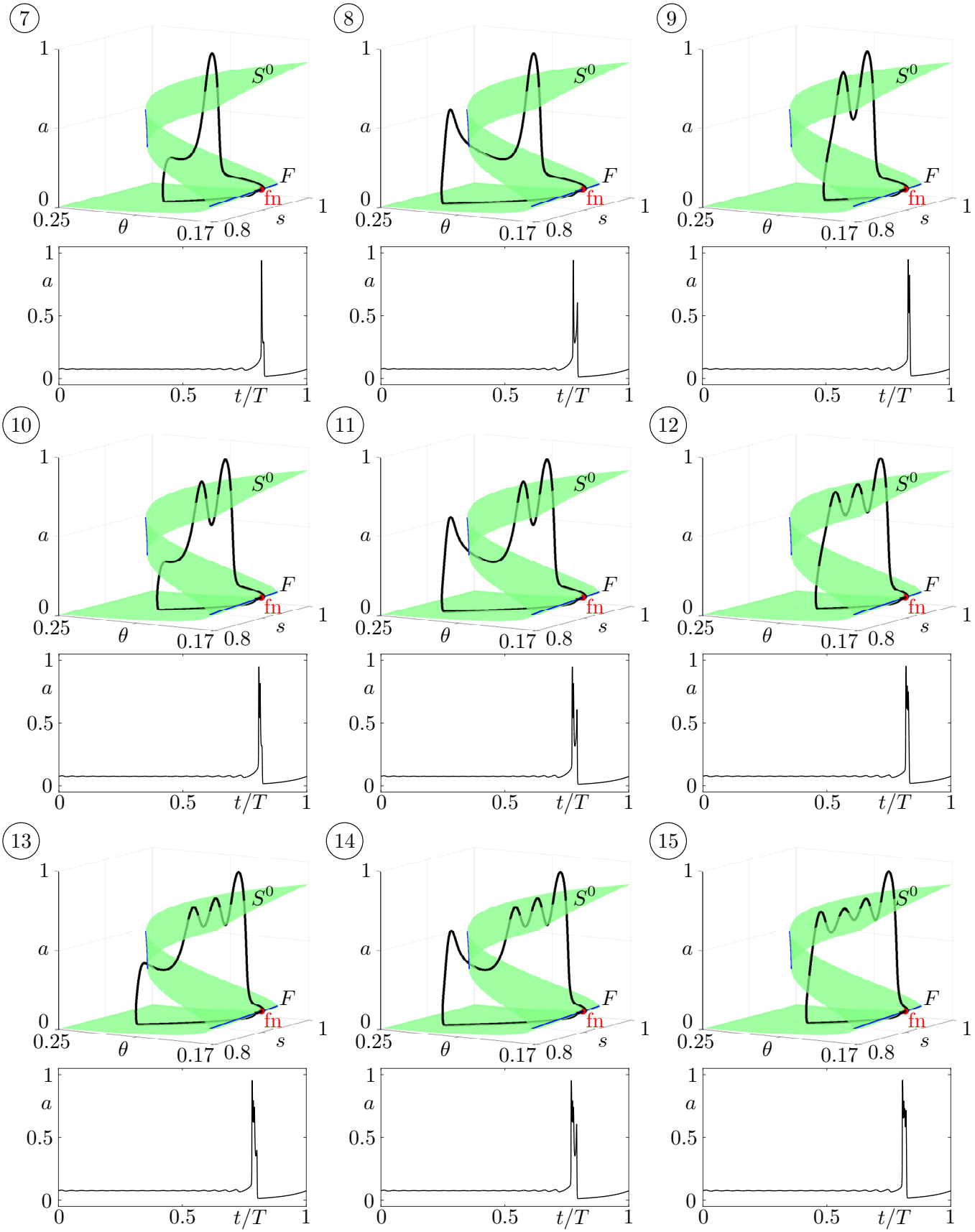

Figure 16: The second, third and fourth canard-mediated spikes along the isola corresponding to MMBO solutions with 17 SAOs. Each up-down pair shows the solution on the (θ, s, a)-space (upper panel) and the time corse of the solution (lower panel). The green surface is the critical manifold S^0 and the blue curve is the lower fold F, the red dot marks the folded node fn.

available data are too scarce to formulate hard conclusions, however we believe that the question deserves to be posed and we propose a deterministic framework to understand the basic mechanisms of these subthreshold fluctuations.
A key parameter in our bifurcation analysis is the level of connectivity within the network, directly related to development of the chick spinal cord. It has been shown that changes in the connectivity affect the duration of both bursting and silent states (see for instance Fig. 13 in [37]). Our dissection of the bifurcation structure of MMBOs reveals as well the emergence of a complex substructure for intermediate connectivity levels: the control on the families of isolas allows to match in a precise way the connectivity parameter with the number of spikes in the burst and the number of SAOs.
Overall, the main interest of the slow-fast approach developed in the present work lies in its ability to map the boundaries between different activity regimes (pure spiking, spiking with subthreshold oscillations, bursting, bursting with subthreshold oscillations, etc.) and different oscillatory patterns within each regime. These are understood through a theoretical prism which allows to identify the organising centres of these boundaries (folded singularities, maximal canards) as well as key (combinations of) parameters to control them (e.g. the number of rotation sectors near a folded node).
Another important novelty of the work is that it provides one of the first studies of canard-induced complex oscillations in rate models. Several follow-up directions can be envisaged. First, coupling general excitatory networks to inhibitory ones and analysing similar slow-fast complex oscillatory dynamics in the resulting E/I systems. In particular, it will be interesting to investigate how multiple-timescales interactions between the different components of such coupled systems may provoke a sudden break-up of the E/I balance, known to trigger transitions to certain pathological brain states (such as epileptic seizures). The same paradigm can be also useful to understand phenomena like the emergence of bursting activity in connected neuronal sub-populations, see [4], or the change in network dynamics related to changes in the effectiveness of synaptic depression, see [1]. In particular, how dynamics of a network can turn from up- and down-states into asynchronous states while increasing the strength of short-term depression. Another future direction will consist in finding a similar slow-fast taxonomy of canard-induced complex oscillations in networks of spiking neurons and compare them with the rate activity that we have observed here.

References

[1] J.M. Benita, A. Guillamon, G. Deco, and M.V. Sanchez-Vives. Synaptic depression and slow oscillatory activity in a biophysical network model of the cerebral cortex. *Frontiers in Computational Neuroscience*, 6:64, 2012.

[2] E. Benoît, J.-L. Callot, F. Diener, and M. Diener. Chasse au canard. *Collect. Math.*, 32(1-2):37–119, 1981.

[3] R. Bertram, J. Rhoads, and W. P. Cimbora. A phantom bursting mechanism for episodic bursting. *Bulletin of Mathematical Biology*, **70**(7):1979–1993, 2008.

[4] M. Bisio, A. Bosca, V. Pasquale, L. Berdondini, and M. Chiappalone. Emergence of bursting activity in connected neuronal sub-populations. *PLOS ONE*, 9(9):1–14, 09 2014.

[5] M Brøns, M. Krupa, and M. Wechselberger. Mixed-mode oscillations due to the generalized canard mechanism. *Fields Inst. Commun.*, 49:39–63, 2006.

[6] J. Burke, M. Desroches, A. M. Barry, T. J. Kaper, and M. A. Kramer. A showcase of torus canards in neuronal bursters. *J. Math. Neurosci.*, 2(3), 2012.

[7] P. De Maesschalck and M. Desroches. Numerical continuation techniques for planar slow-fast systems. *SIAM J. Appl. Dyn. Syst.*, 12(3):1159–1180, 2013.

[8] M. Desroches, J. Guckenheimer, B. Krauskopf, C. Kuehn, H. M. Osinga, and M. Wechselberger. Mixed-mode oscillations in a multiple time scale. *SIAM Rev.*, 54(2):211–288, 2012.

[9] M. Desroches, T. J. Kaper, and M. Krupa. Mixed-mode bursting oscillations: Dynamics created by a slow passage through spike-adding canard explosion in a square-wave burster. *Chaos*, 23:046106, 2013.

[10] M. Desroches, M. Krupa, and S. Rodrigues. Inflection, canards and excitability threshold in neuronal models. *J. Math. Biol.*, 67:989–1017, 2013.

[11] M. Desroches, M. Krupa, and S. Rodrigues. Spike-adding in parabolic bursters: The role of foded-saddle canards. *Physica D*, 331:58–70, 2016.

[12] B. Ermentrout and D.H. Terman. *Mathematical Foundations of Neuroscience*. Springer, 2010.

[13] B. Fedirchuk, P. Wenner, P. Whelan, S. Ho, J. Tabak, and M. J. O'Donovan. Spontaneous network activity transiently depresses synaptic transmission in the embryonic chick spinal cord. *J. Neurosci.*, 19:2102–2112, 1999.

[14] N. Fenichel. Asymptotic stability with rate conditions II. *Indiana Univ. Math. J.*, 26:81–93, 1977.

[15] J. Guckenheimer and C. Kuehn. Computing slow manifolds of saddle type. *SIAM J. Appl. Dyn. Syst.*, 8(3):854–879, 2009.

[16] E. M. Izhikevich. Neuronal excitability, spiking and bursting. *Int. J. Bifur. and Chaos*, 10(6):1171–1266, 2000.

[17] J. Jalics, M. Krupa, and H. G. Rotstein. Mixed-mode oscillations in a three time-scale system of odes motivated by a neuronal model. *Dyn. Syst.*, 25(4):445–482, 2010.

[18] E. Köksal Ersöz, M. Desroches, and M. Krupa. Synchronization of weakly coupled canard oscillators. *Physica D*, 349:46–61, 2017.

[19] E. Köksal Ersöz, M. Desroches, C. R. Mirasso, and S. Rodrigues. Anticipation via canards in excitable systems. submitted, 2018.

[20] M. A. Kramer, R. D. Traub, and N. Kopell. New dynamics in cerebellar purkinje cells: torus canards. *Phys. Rev. Lett.*, 101(6):068103, 2008.

[21] M. Krupa, N. Popovic, N. Kopell, and H. G. Rotstein. Mixed-mode oscillations in a three time-scale model for the dopaminergic neuron. *Chaos*, 18(49):015106, 2008.

[22] M. Krupa and P. Szmolyan. Relaxation oscillation and canard explosion. *J. Differ. Equ.*, 174(2):312–368, 2001.

[23] J. Mitry, M. McCarthy, N. Kopell, and M. Wechselberger. Exitable neurons, firing threshold manifolds and canards. *J. Math. Neurosci.*, 3(12), 2013.

[24] J. Moehlis. Canards for a reduction of Hodgkin-Huxley equations. *J. Math. Biol.*, 52:141–153, 2006.

[25] J. Nowacki, H. M. Osinga, and K. Tsaneva-Atanasova. Dynamical systems analysis of spike-adding mechanisms in transient bursts. *J. Math. Neurosci.*, 2(7), 2012.

[26] M. J. O'Donovan. The origin of spontaneous activity in developing networks of the vertebrate nervous system. *Curr. Opin. Neurobiol.*, 9:94–104, 1999.

[27] M. J. O'Donovan and N. Chub. Population behavior and self-organization in the genesis of spontaneous rhythmic activity by developing spinal networks. *Semin. Cell Dev. Biol.*, 8:21–28, 1997.

[28] H. M. Osinga and K. Tsaneva-Atanasova. Dynamics of plateau bursting in dependence on the location of its equilibrium. *J. Neuroendocrinol.*, 22(12):1301–1314, 2012.

[29] J. Rinzel. Bursting oscillations in an excitable membrane model. In B. D. Sleeman and R. J. Jarvis, editors, *Ordinary and partial differential equations (Proceedings of the Eighth Conference held at Dundee, Scotland, June 25-29, 1984)*, volume **1511** of *Lecture Notes in Mathematics*, pages 304–316. Springer, 1985.

[30] J. Rinzel. A formal classification of bursting mechanisms in excitable systems. In *International Congress of Mathematicians, Berkeley, California, USA, August 3-11, 1986*, volume II, pages 1578–1593. American Mathematical Society, 1987.

[31] J. Rinzel. A formal classification of bursting mechanisms in excitable systems. In E. Teramoto and M. Yumaguti, editors, *Mathematical topics in population biology, morphogenesis and neurosciences (Proceedings of an International Symposium held in Kyoto, November 10-15, 1985)*, volume **71** of *Lecture Notes in Biomathematics*, pages 267–281. Springer, 1987.

[32] J. Rubin and M. Wechselberger. Giant squid-hidden canard: the 3D geometry of the Hodgkin-Huxley model. *Biol. Cybern.*, 97:5–32, 2007.

[33] J. Rubin and M. Wechselberger. The selection of mixed-mode oscillations in a Hodgkin-Huxley model with multiple timescales. *Chaos*, 18:015105, 2008.

[34] P. Szmolyan and M. Wechselberger. Canards in $\mathbb{R}^3$. *J. Differ. Equ.*, 177:419–453, 2001.

[35] J. Tabak, M. J. O'Donovan, and J. Rinzel. Differential control of active and silent phases in relaxation models of neuronal rhythms. *J. Comput. Neurosci.*, 21(3):307–328, 2006.

[36] J. Tabak, W. Senn, and M. J. O'Donovan. The role of activity-dependent network depression in the expression and self-regulation of spontaneous activity in the developing spinal cord. *J. Neurosci.*, 21(22):8966–8978, 2001.

[37] J. Tabak, W. Senn, M. J. O'Donovan, and J. Rinzel. Modeling of spontaneous activity in developing spinal cord using activity-dependent depression in an excitatory network. *J. Neurosci.*, 20(8):3041–3056, 2000.

[38] D. Terman. Chaotic spikes arising from a model of bursting in excitable membranes. *SIAM J. Appl. Math.*, 51(5):1418–1450, 1991.

[39] K. Tsaneva-Atanasova, H. M. Osinga, T. Riess, and A. Sherman. Full system bifurcation analysis of endocrine bursting models. *J. Theor. Biol.*, 284(4):1133–1146, 2010.

[40] M. Wechselberger. Existence and bifurcation of canards in $\mathbb{R}^3$ in the case of a folded node. *SIAM J. Appl. Dyn. Syst.*, 4(1):101–139, 2005.